ρ_p = particle density, g/cm^3
τ = time, min or h
φ = factor due to diffusional resistance through product layer, Eq. 8
ω = weight ratio, $CaCO_3/MgCO_3$

LITERATURE CITED

Borgwardt, R. H., "Kinetics of the Reaction of SO_2 with Calcined Limestone," *Environ. Sci. Tech.*, 4(1), p. 59 (1970).

Borgwardt, R. H., and R. D. Harvey, "Properties of Carbonate Rocks Related to SO_2 Reactivity," *Environ. Sci. Tech.*, 6(4), p. 350 (1972).

Borgwardt, R. H., Private Communication (1983).

Chrostowski, J. W., and C. Georgakis, "Pore Plugging Model for Gas-Solid Reactions," *ACS Symp. Ser.*, **65**, p. 225 (1978).

Coutant, R. W., R. E. Barrett, R. Simon, B. E. Campbell, and E. H. Lougher, "Investigation of the Reactivity of Limestone and Dolomite for Capturing SO_2 from Flue Gas," Summary Report, Batelle Memorial Inst. for the Nat. Pollution Control Adm., Publication No. PB-196749 (Nov. 20, 1970).

Doğu, T., "The Importance of Pore Structure and Diffusion in the Kinetics of Gas-Solid Noncatalytic Reactions: Reaction of Calcined Limestone with SO_2," *Chem. Eng. J.*, **21**, p. 213 (1981).

Hartman, M., and O. Trnka, "Influence of Temperature on the Reactivity of Limestone Particles with Sulfur Dioxide," *Chem. Eng. Sci.*, **35**, p. 1189 (1980).

Hartman, M., J. Hejna, and Z. Beran, "Application of the Reaction Kinetics and Dispersion Model to Gas-Solid Reactors for Removal of Sulfur Dioxide from Flue Gas," *Chem. Eng. Sci.*, 34, p. 475 (1979).

Hartman, M., "Comparison of various carbonates as absorbents of sulfur dioxide from combustion gases," *Int. Chem. Eng.*, 18(4), p. 712 (1978b).

Hartman, M., and R. W. Coughlin, "Reaction of Sulfur Dioxide with Limestone and the Grain Model," *AIChE J.*, **22**(3), p. 490 (1976).

Hartman, M., J. Pata, and R. W. Coughlin, "Influence of Porosity of Calcium Carbonates on Their Reactivity with Sulfur Dioxide," *Ind. Eng. Chem. Process Des. Dev.*, **17**(4), p. 411 (1978a).

Hartman, M., and R. W. Coughlin, "Reaction of Sulfur Dioxide with Limestone and the Influence of Pore Structure," *Ind. Eng. Chem. Process Des. Dev.*, **13**(3), p. 248 (1974).

Lee, D. C., and C. Georgakis, "A Single, Particle-Size Model for Sulfur Retention in Fluidized Bed Coal Combustors," *AIChE J.*, **27**, p. 472 (1981).

Pigford, R. L., and G. Sliger, "Rate of Diffusion-Controlled Reaction Between a Gas and a Porous Solid Sphere:Reaction of SO_2 with $CaCO_3$," *Ind. Eng. Chem. Proc. Des. Dev.*, **12**(1), p. 85 (1973).

Reid, W. T., "Basic Factors in the Capture of Sulfur Dioxide by Limestone and Dolomite," *J. of Eng. for Power, Trans. ASME*, Ser. A, **92**(1), p. 11 (1970).

Vogel, G. J., et al., "Supportive Studies in Fluidized-Bed Combustion," Argonne Nat. Lab. Report for U.S. Energy Res. and Dev. Adm. and U.S. EPA, ANL/ES-CEN-1019 and FE-1780-7 (April, 1977).

Manuscript received December 20, 1982; revision received May 2, and accepted May 10, 1983.

Breakage Functions for Droplets in Agitated Liquid-Liquid Dispersions

Photographic measurements of transient drop-size distributions from stirred liquid-liquid systems of low dispersed phase fraction in a batch vessel confirm consistency with a similarity behavior from population balance established earlier by Narsimhan et al. (1980). Moreover, breakage functions are presented in generalized dimensionless form accounting for dependence on physical properties of the system and power input through stirring. This information is essential for predicting drop-size distributions in stirred liquid-liquid systems. Experimental measurements of steady-state drip-size distributions obtained from stirred, continuous flow systems with known inlet drop sizes compare very favorably with theoretical predictions based on population balance analysis using the breakage functions obtained from batch experiments.

GANESAN NARSIMHAN, GREGORY NEJFELT, and DORAISWAMI RAMKRISHNA

School of Chemical Engineering
Purdue University
West Lafayette, IN 47907

SCOPE

Prediction of rate processes in stirred liquid-liquid systems should account not only for the rate processes occurring in single droplets but also for the dynamics of drop breakage and coalescence responsible for the evolution of the drop population. This can be accomplished by the application of the population balance framework to such systems, the success of which hinges on proper identification of certain functions necessary for the description of drop breakage and coalescence. In stirred dispersions, drop breakage can be characterized by: (i) the rate function for drop breakage and (ii) the size distribution of daughter droplets formed upon the breakage of a parent droplet.

The present work builds on past efforts of Narsimhan et al. (1980) to determine the breakage functions by batch experiments in which drop-size distributions are measured experimentally (by photographic means in the present work) through the aid of a mathematical similarity theory. The breakage functions so obtained are characterized by physical properties of the system and parameters governing the rate of stirring and the vessel geometry.

The veracity of the foregoing information is tested by continuous flow experiments in which feed drop sizes are known and comparing the measured steady-state distributions with those predicted by population balance theory.

Correspondence concerning this paper should be addressed to D. Ramkrishna.

CONCLUSIONS AND SIGNIFICANCE

Experimental data on the transients of drop-size distributions in batch stirred liquid-liquid dispersions of low dispersed phase fraction for three different dispersed phases obtained through high-speed macrophotography are found to be consistent with a similarity behavior from population balances established earlier by Narsimhan et al. (1980). The rate functions for breakage calculated from the experimental data within the similarity framework, when nondimensionalized with the natural frequency of oscillation of droplets give a very satisfactory generalized plot against the dimensionless drop volume ratio $(v/L^3)^{5/9}We$.

The estimated daughter droplet distribution functions indicate that breakage is not "thorough" and that "erosive" breakage may be more common. However, consistent with the concept of similarity, larger drops break more "thoroughly" than small drops. The expression for the cumulative volume fraction of daughter droplets relative to the parent drop size is obtained, as a result of the underlying similarity theory, in terms of the ratio of the breakage rates of daughter and parent droplets. The correlation we present acquires a universal form in that it is free of the parameters appearing in the breakage rate.

Experimental measurements of the steady-state drop-size distribution in a stirred continuous flow system with known inlet drop sizes in the average residence time range of 60 to 360 s generally compare very well with the theoretical predictions based on population balance analysis using the breakage functions obtained from batch experiments. It is shown that the steady-state drop-size distributions in such continuous flow systems would exhibit a similarity behavior in terms of the similarity variable $\Gamma(v)\theta$ when the average residence time is much greater than the time scale of breakage of inlet droplets. The experimental steady-state drop-size distributions substantiate the proposed similarity behavior.

The information in this paper could be valuable for the prediction of breakage functions in stirred liquid-liquid dispersions necessary for the analysis of rate processes in such systems whenever the dynamic droplet phenomena play an important role.

INTRODUCTION

Analysis of rate processes in dispersed-phase systems must account both for the dynamic state of the dispersed-phase population and rate processes occurring in single particles. The population balance framework is essential to this task. Narsimhan, Ramkrishna and Gupta (1980) have recently discussed the problem at length with specific reference to stirred liquid-liquid dispersions. The problem of predicting drop-size distributions through the population balance framework is traced to that of determining the breakage and coalescence rates of droplets under conditions prevailing in the stirred vessel. In lean dispersions, the dispersed-phase fraction is small enough to neglect the effect of coalescence at early stages of the evolution of drop-size distributions in a batch system. Transient measurements of drop-size distributions in such systems should therefore serve to obtain information about droplet breakage. Information about drop breakage pertains to the breakage rate of single droplets as well as the size distribution of daughter droplets arising from a given breakage. Narsimhan et al. (1980) used a certain similarity theory to obtain the breakage rate of single drops as a function of drop size. However, for several reasons, the above work required further reinforcement. First, the data on transient drop-size distributions were obtained by using an encapsulation technique, which because of its essentially invasive nature could be suspect. Second, the transition probability was obtained only up to a multiplicative constant. Third, the daughter drop-size distribution was not obtained. It is therefore the objective of this paper to: (i) reconfirm the applicability of the similarity analysis of Narsimhan et al (1980) by using a direct (noninvasive) photographic technique for drop-size distributions; (ii) obtain the absolute breakage rate and the daughter droplet-size distribution and characterizing the same by generalized dimensionless groups accounting for system properties and power input through stirring; and (iii) use the foregoing information for predicting steady-state drop-size distributions in a continuous-flow stirred vessel with specified feed-size distribution and to compare them with measured drop-size distributions as a further means of validating the identified breakage functions.

THEORY

We let $F(v,t)$ be the cumulative volume fraction at time t of drops with volumes less than or equal to v. Then the evolution of drop-size distributions in a batch stirred vessel with negligible coalescence is described by

$$\frac{\partial}{\partial t}F(v,t) = \int_v^\infty \Gamma(v')G(v,v')\partial_v F(v',t) \tag{1}$$

where $\Gamma(v)$ is the breakage rate of drops of volume v; $G(v,v')$ is the cumulative volume fraction of daughter droplets with volumes less than or equal to v arising from the breakage of a parent drop with volume v'. The basis for similarity behavior is contained in assuming that $G(v,v')$ is of the form

$$G(v,v') = g\left(\frac{\Gamma(v)}{\Gamma(v')}\right) \tag{2}$$

and has been discussed at length by Narsimhan et al. (1980). Briefly, we observe here that the form (Eq. 2) is inspired by the hypothesis that larger drops break more thoroughly (in the sense that many daughter droplets may be formed) than smaller droplets which break into relatively fewer droplets. The merit of the form (Eq. 2) lies in its admitting a similarity solution to Eq. 1 of the form

$$F(v,t) = f(z), \qquad z = \Gamma(v)t \tag{3}$$

Then Eq. 1 leads to the integral equation

$$\phi(z) = \int_z^\infty g\left(\frac{z}{\zeta}\right)\phi(\zeta)d\zeta \tag{4}$$

where $\phi(z) \equiv zdf/dz$. Narsimhan et al. (1980) have pointed out that an experimental test of the applicability of Eq. 3 is to examine a plot of lnt vs. lnv at various fixed values of volume fraction F. If the curves for lnt (along the ordinate) vs. lnv (along the abscissa) for different volume fractions F can be collapsed into a single curve by a vertical translation, then the similarity hypothesis is upheld. Mathematically, one obtains

$$\frac{dln\,\Gamma(v)}{dlnv} = -\left(\frac{\partial lnt}{\partial lnv}\right)_F \tag{5}$$

for the details of which we refer to Narsimhan et al. (1980). Clearly, the collapsed curve provides the transition probability $\Gamma(v)$ up to a multiplicative constant because integration of Eq. 5 yields

$$\Gamma(v) = \Gamma(v_o)\exp\left[-\int_{lnv_o}^{lnv}\left(\frac{\partial lnt}{\partial lnv}\right)_F dlnv\right] \tag{6}$$

in which v_o is some reference volume. The experiments reported

by Narsimhan et al. (1980) upheld the concept of similarity and the transition probability as determined by Eq. 6 was obtained up to the multiplicative constant $\Gamma(v_o)$. By redefining the similarity variable as $z' \equiv \Gamma(v)t/\Gamma(v_o)$, the function $f(z)$ in Eq. 3 as $\tilde{f}(z')$, Eq. 4 may be replaced by

$$\tilde{\phi}(z') = \Gamma(v_o) \int_{z'}^{\infty} g\left(\frac{z'}{\zeta'}\right) \tilde{\phi}(\zeta')d\zeta' \tag{7}$$

where $\tilde{\phi}(z') = z'd\tilde{f}/dz'$. A further check on the similarity can be seen in a plot of $\tilde{f}(z')$ vs. z' which would display all the transient drop-size distributions in a single curve (Narsimhan et al., 1980). We define moments

$$\mu_n \equiv \int_o^{\infty} z'^n \frac{df}{dz'} dz' \qquad n = 1, 2, \ldots \tag{8}$$

$$\nu_n \equiv \int_o^1 x^n g(x)dx \qquad n = 0, 1, 2, \ldots . \tag{9}$$

Equation 7 may be multiplied by z'^{n-1} and integrated with respect to z' between o and ∞ to obtain

$$\Gamma(v_o)\nu_{n-1} = \frac{\tilde{\mu}_n}{\tilde{\mu}_{n+1}}, \qquad n = 1, 2, \ldots . \tag{10}$$

The procedure as suggested by Narsimhan et al. (1980) (see also Ramkrishna, 1974) to calculate $\Gamma(v_o)$ and the function g was to solve for the $\Gamma(v_o)g$ in terms of its moments obtained by computing the moments $\{\mu_n\}$ from the similarity plot of $\tilde{f}(z')$ vs. z'. This procedure was not done by Narsimhan et al. (1980) however on their data. In the present work, an effort made in this direction led to considerable difficulties. The difficulties arise from the practical necessity to truncate the integral in Eq. 7 at the upper limit which *cannot* admit a nontrivial solution for $\tilde{\phi}$ since the truncated equation would be a homogeneous Volterra integral equation. It must be recognized however that Eq. 7 is capable of admitting a nontrivial solution with the upper limit retained as ∞. Since the experimental data showed a tendency for $\tilde{f}(z')$ to level off to its maximum value of unity for relatively finite values of z' (instead of ∞) it implies that $\tilde{\phi}(z')$ must vanish for finite values of z'. Examining the right hand side of Eq. 7, one must conclude that $g(z'/\zeta')$ must vanish for some lower limit x_o of the fraction z'/ζ'. Physically this means that the volume fraction of droplets of volume less than a fraction x_o of the parent drop volume should be zero. Equation 7 would then become

$$\tilde{\phi}(z') = \Gamma(v_o) \int_{z'}^{z'/x_o} g\left(\frac{z'}{\zeta'}\right) \tilde{\phi}(\zeta')d\zeta' \tag{11}$$

which is not subject to the constraint of a trivial solution referred to earlier. Our attempts to solve Eq. 11 met with many numerical difficulties. We therefore resorted to an alternative approach predicated on g being a Beta-distribution which consists of three parameters. Thus

$$g(x) = \frac{(r+s-1)!}{(r-1)!(s-1)!} \int_o^{(x-x_o)/(1-x_o)} \xi^r(1-\xi)^s d\xi \tag{12}$$

where the factorials must be interpreted in terms of the Gamma function since r and s are not necessarily integers. The parameters x_o, r, s and $\Gamma(v_o)$ were estimated by an unconstrained multivariate optimization scheme using Eq. 10. We refer to the Appendix for details.

The identification procedure is essentially complete at this stage. It should, in principle, be possible also to determine the *mean* number of daughter droplets, $\nu(v')$, arising from the breakage of a parent droplet of volume v' since

$$\nu(v') = \int_0^{v'} \left(\frac{v'}{v}\right) \frac{\partial G}{\partial v}(v,v')dv \tag{13}$$

If one accepts the existence of a maximum stable drop volume v_s below which drops retain their size without breakage in the flow field (Levich, 1962; Shinnar, 1961), then $\Gamma(v) = 0$ for $v < v_s$. Rewriting Eq. 13

$$\nu(v') = \int_0^{v_s} \left(\frac{v'}{v}\right) \frac{\partial G}{\partial v}(v,v')\,dv + \int_{v_s}^{v'} \left(\frac{v'}{v}\right) \frac{\partial G}{\partial v}(v,v')dv \tag{14}$$

Note that although drops of volume less than v_s cannot break they may be formed upon breakage of larger droplets. The proposed concept of similarity cannot be reconciled within the drop volume range $0 < v < v_s$, because $\Gamma(v_s) = 0$ and that would imply that $G(v,v') = 0$ for $v < v_s$. It is contended that daughter droplets of volume less than v_s are of *negligible volume*, but insofar as they may represent considerable *numbers*, we may not neglect the first term on the righthand side of Eq. 14. By letting $\nu_s(v')$ represent the mean number of daughter droplets (from the breakage of a droplet of volume v') with volume less than v_s, we may write Eq. 14 as

$$\nu(v') - \nu_s(v') = \int_{v_s}^{v'} \left(\frac{v'}{v}\right) \frac{\partial G}{\partial v}(v,v')dv \tag{15}$$

Using Eq. 2, Eq. 15 may be further rewritten as

$$\nu(v') - \nu_s(v') = \int_0^1 \frac{v'}{\Gamma^{-1}(x\Gamma(v'))} g'(x)dx \tag{16}$$

The function Γ^{-1} in Eq. 16 is defined as the inverse mapping of $\Gamma(v)$, i.e., $\Gamma^{-1}(\Gamma(v)) = v$. Since drop volume measurements could not extend to very small droplets, our experiments cannot be expected to yield the values of $\nu_s(v')$. Estimates of the righthand side of Eq. 16 can be made from the identified functions $\Gamma(v)$ and $g(x)$. [From Eq. 16 it is possible to deduce that as $v' \to v_s$, $\nu(v_s) = 1 + \nu_s(v_s)$ which is a mathematical abstraction of the "breakage" of a droplet of volume v_s into itself and $\nu_s(v_s)$ others of zero volume.]

We now turn our attention to the equations governing a continuous flow vessel with a specified feed drop-size distribution. The dispersion is assumed to be perfectly stirred and that the effluent drop-size distribution is identical to that in the vessel at any instant. The function $F(v,t)$ should satisfy the equation

$$\frac{\partial F}{\partial t}(v,t) = \frac{1}{\theta}[F_f(v) - F(v,t)] + \int_v^{\infty} \Gamma(v')G(v,v')\partial_v F(v',t) \tag{17}$$

where $F_f(v)$ is the cumulative volume fraction of droplets in the feed which is presumed to be known. The steady state version of Eq. 17 yields

$$\tilde{F}(v) = F_f(v) + \theta \int_v^{\infty} \Gamma(v')G(v,v')\partial_v \tilde{F}(v') \tag{18}$$

With a view to solving Eq. 18 let us write the feed distribution $F_f(v)$ as

$$F_f(v) = \int_0^{\infty} S(v - v_f)dF_f(v_f) \tag{19}$$

where $S(x)$ is the step function defined by

$$S(x) = \begin{cases} 1 & x > 0 \\ 0 & x < 0 \end{cases}$$

The advantage in expressing $F_f(v)$ as in Eq. 19 lies in the fact that Eq. 18 can be solved readily in the discretized form for the feed distribution $S(v - v_f)$ which corresponds to identically sized inlet drops of volume v_f. Suppose the solution to this problem (to be established presently) is denoted by $F(v,v_f)$; i.e., $F(v;v_f)$ satisfies the equation

$$F(v;v_f) = S(v - v_f) + \theta \int_v^{\infty} \Gamma(v')G(v,v')dF(v';v_f) \tag{20}$$

Then the solution to Eq. 18 may be identified as

$$\tilde{F}(v) = \int_0^{\infty} F(v;v_f)dF_f(v_f) \tag{21}$$

which follows from the linearity of Eq. 18. Equation 20 may be

solved by discretizing the drop volume interval. First we recognize that in this case droplets of volume larger than v_f cannot appear in the vessel by breakage so that we need only be concerned with the interval $[0,v_f]$. Thus we may divide $[0,v_f]$ into N equal intervals with

$$v_i = \frac{iv_f}{N}, \qquad i = 0, 1, 2, \ldots N$$

Letting $F_i(v_f) = F(v_i;v_f)$, $\Gamma_j = \Gamma(v_j)$, $G_{ij} = G(v_iv_j) = g(\Gamma_i/\Gamma_j)$ we have the solution

$$F_N(v_f) = 1$$

$$F_i(v_f) = \theta \sum_{j=i}^{N-1} \Gamma_j G_{ij}[F_{j+1}(v_f) - F_j(v_f)]$$

$$i = 1, 2 \ldots, (N-1) \quad (22)$$

The solution to Eq. 18, expressed in the form 21 may then be identified by a suitably discretized version of Eq. 21. Thus the steady-state distribution can be predicted using the values of the functions Γ and g, which can be compared with experimentally measured distributions.

In the foregoing analysis, no consequences of the similarity behavior observed in batch systems, were implied in the determination of the steady-state drop-size distribution which depended on the feed-size distribution. In this regard, it is interesting to ponder the possibility of whether a similarity behavior of any sort may manifest in the continuous flow system. Such behavior may produce a steady-state distribution relatively insensitive to the feed distribution. This would be especially convenient because frequently, the feed to such systems is in the form of large drops whose sizes are unknown and will undergo virtually instantaneous breakage into droplets of unknown size. Each individual drop entering the system would give rise to a population of its progeny which could display similarity behavior excepting for the loss occurring due to droplets leaving with the exit stream. Of course, in a perfectly stirred system, droplets (free from significant buoyancy effects) would leave sooner with higher probability so that the manifestation of similarity depends on the magnitude of the time scale in which similarity behavior is attained relative to that of drops leaving the system. For larger average residence times (for low flow rates) the volume fraction of drops leaving before similarity behavior manifests is possibly small. Conversely, at smaller average residence times one may not expect similarity behavior. In what follows we present a mathematical treatment of the foregoing considerations.

Consider the situation following entry of any feed drop into the system at some time arbitrarily set equal to zero. Thereupon we follow the evolution of its progeny along time denoted by τ. In the following, it is most convenient to allow the daughter droplets to inherit the age of their parent so that the progeny of a single antecedent (which originally entered the vessel) is identified by their common age. Thus we define a function $F(v,\tau)$ such that $F(v,\tau)d\tau$ is the *cumulative volume* fraction of droplets with age between τ and $\tau + d\tau$ at steady state. Indeed

$$\tilde{F}(v) = \int_0^\infty \tilde{F}(v,\tau)d\tau \quad (23)$$

It is readily seen that $\tilde{F}(v,\tau)$ must satisfy

$$\frac{\partial \tilde{F}}{\partial \tau}(v,\tau) = -\frac{1}{\theta}F(v,\tau) + \int_v^\infty \Gamma(v')G(v,v')\partial_{v'}\tilde{F}(v',\tau) \quad (24)$$

which may be rewritten as

$$\frac{\partial}{\partial \tau}[\tilde{F}(v,\tau)e^{\tau/\theta}] = \int_v^\infty \Gamma(v')G(v,v')\partial_{v'}\tilde{F}(v',\tau)e^{\tau/\theta} \quad (25)$$

Switching to a new age variable $\tau' \equiv \tau/\theta$, and representing $\tilde{F}'(v,\tau') = \theta\tilde{F}(v,\tau)$ we convert Eq. 25 to

$$\frac{\partial}{\partial \tau'}[\tilde{F}'(v,\tau')e^{\tau'}] = \theta \int_v^\infty \Gamma(v')G(v,v')\partial_{v'}[\tilde{F}'(v',\tau)e^{\tau'}] \quad (26)$$

Equation 26 is of the same form as Eq. 1 so that when Eq. 2 is true we expect a similarity solution of the form

$$\tilde{F}'(v,\tau')e^{\tau'} = f(\theta\Gamma(v)\tau') \quad (27)$$

for *large enough* τ'. We interpret "large" τ' as that which satisfies that condition

$$\tau' \gg \frac{1}{\theta\Gamma(v_f)}$$

where v_f is the volume of a typical feed droplet. Clearly if $\Gamma(v_f)\theta \gg 1$, we expect Eq. 27 to be satisfied for reasonably *small* values of τ'. This conclusion is important in what follows. Rewriting Eq. 23 as

$$\tilde{F}(v) = \int_0^\infty \tilde{F}'(v,\tau')d\tau'$$

$$\approx \int_0^\infty f(\theta\Gamma(v)\tau')e^{-\tau'}d\tau'$$

which is a function of $\theta\Gamma(v)$ thus implying a similarity behavior with the variable $\theta\Gamma(v)$. This result is found to be substantiated by our experimental data discussed later in the paper.

EXPERIMENTAL DETAILS

Experimental measurements of drop-size distributions were made for three different dispersed phases: (i) Chlorobenzene, (ii) CCl_4 i-octane mixture (0.5–0.5), and (iii) Anisole CCl_4 mixture (0.8–0.2). In all the experiments, the continuous phase was distilled water presaturated with the dispersed phase. Presaturation was necessary to prevent mass transfer during the experiment. The physical properties of the dispersed phases are given in Table 2 of Narsimhan et al. (1980).

Batch Experiments

Batch experiments were conducted in a 2×10^{-3} m^3 flanged glass vessel, 0.13 m in diameter, 0.14 m high. The glass vessel was fitted with optical windows for photographing the dispersion. The optical windows were circular, 0.05 m in diameter, made of high-quality plane optical glass and were fixed at 0.07 m from the bottom of the vessel. While fixing the optical windows to the vessel, care was taken to avoid sharp corners to minimize dead zones in the vessel. The vessel was filled with liquid-liquid dispersion to a height of 0.13 m and was immersed in a rectangular perspex water bath to maintain constant temperature during measurements. All experiments were conducted at 300 ± 0.1 K. The rectangular water bath was also fitted with optical glass windows of the same dimensions as that of the vessel. The liquid-liquid mixture was agitated by means of a six-blade stainless-steel turbine impeller of 0.05 m diameter. The impeller was located 0.03175 m from the vessel bottom. Four stainless-steel baffles 0.14 m long, 0.013 m wide and 3.125×10^{-3} m thick were equally spaced at 90° perpendicular to and 6.35×10^{-3} m away from the vessel wall. The details of the mixing vessel assembly are given in Figure 1. The agitator was driven by Fischer stedi-speed stirrer with speed control. The experiments were conducted at three agitator speeds, 5 s^{-1}, 6.67 s^{-1} and 8.33 s^{-1}.

The drop-size distributions were determined by macrophotography (high magnification photography) of the dispersion through the optical windows. Olympus OM-2(N) 35 mm camera with autobellows and 80 mm f4 zuiko macrolens was used for this purpose. The dispersion was illuminated by General Radio Type 1538-A Strobotac. The schematic diagram of the arrangement is shown in Figure 2. The mixing vessel assembly was positioned in the perspex water bath, the optical windows of the vessel and the water bath aligned. Back illumination of the dispersion was used to enhance the contrast of the image. The strobotac was positioned such that the full illumination could be viewed through the camera. The length of the bellows was adjusted for a magnification of 1:1. Under such a large magnification, the image has very small depth of field and negligible parallax due to the large distance between the film plane and the plane of focus. Therefore, it is possible to focus virtually on a plane. For a magnification of 1:1, the distance between the film plane and the plane of focus was around 0.25 m. In order to freeze the motion of droplets at the time of measurement, it is necessary to have a flash of very small duration. Furthermore, the flash should be of high intensity for proper exposure of the film. Genrad Strobotac was found to satisfy these requirements fairly well. The flash was located at a distance of 0.23 m from the plane of focus and was operated at high intensity mode. The intensity of the flash was 15×10^6 beam candles and

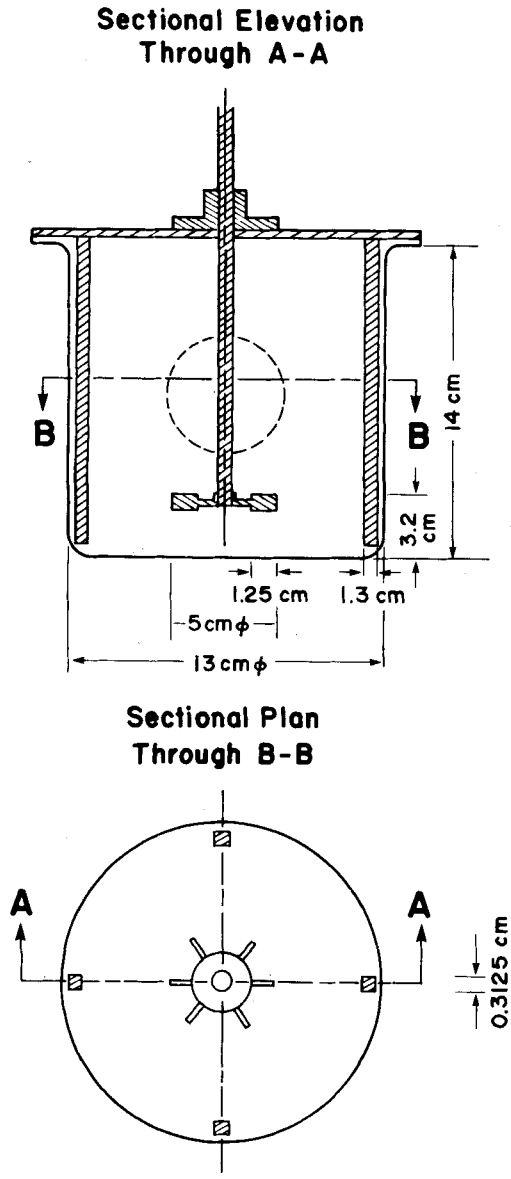

Figure 1. Plan and elevation of mixing vessel.

the flash duration was around 3 microseconds. The camera shutter opening was synchronised with the flash by means of 1531-P2 Genrad delay triggered by the shutter. Since the duration of shutter opening was very much larger than flash duration, the photographs were taken in the dark to avoid stray light falling on the film. Kodak high contrast copy film was found to be satisfactory. The aperture opening of the lens can usually be calculated from the film speed, light intensity of the light source and the distance between the film and the plane of focus. However, in our case, the aperture opening would depend upon the attenuation of light intensity due to the liquid-liquid dispersion. Since the attenuation is proportional to the interfacial area per unit volume of the dispersion, one would expect the aperture setting to change with change in drop size distributions. The aperture opening of the lens for different experimental conditions was ascertained by trial and error by viewing the dispersion through the camera during flashing. If the aperture setting is indeed correct, then one should be able to see sharp shadow images of the drops due to the difference in the refractive indices of the continuous and dispersed phases. The aperture setting varied from f/8 for drop populations at small times to f/4 for large times. The shutter speed was 1 s and the flash delay was maintained at 0.5 s. To insure that the camera was focused onto the same plane in the mixing vessel, a stainless steel wire was lowered into the mixing vessel at a fixed position and the camera focused on the wire. External illumination was found to be necessary at the time of focusing. Drop-size distributions were determined by observing the negatives through a microscope. The drop diameters were measured using a micrometer eyepiece. The magnification of the photograph was calibrated by photographing an ocular scale suspended in the mixing vessel at the plane of focus.

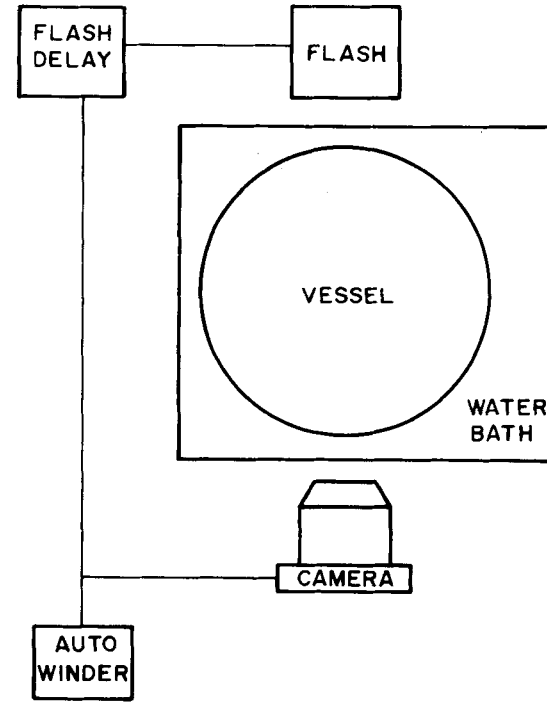

Figure 2. Schematic diagram of the batch experimental setup.

Experimental Procedure

The mixing vessel, the stainless steel baffle assembly and the agitator were cleaned with chromic acid, rinsed thoroughly with distilled water. The vessel was charged with 1.8×10^{-3} m^3 of distilled water presaturated with the dispersed phase. Presaturation was done to avoid mass transfer of the dispersed phase into continuous phase during agitation. It was ensured that the vessel is free of all air bubbles. The mixing vessel assembly was then lowered into the rectangular perspex water bath, positioned to align the optical windows. The speed of the agitator was measured with strobotac and checked for its constancy. The agitation was then stopped. The stainless-steel wire was positioned into the mixing vessel about 0.0125 m from the optical window. The camera was focused onto the stainless-steel wire and the wire removed. The system was allowed to equilibrate until the temperature remains constant at 300 ± 0.1 K. TE-7 Tempette temperature controller was used for this purpose. Dispersed phase was then added to the mixing vessel, the agitation started and photographs taken at different instants of time. The experiment was conducted in a dark room to avoid stray light during photography. The camera was mounted on a tripod and olympus auto-winder was used to avoid disturbing the position of the camera during winding.

A sample of around 300 droplets were counted for each distribution measurement. Drops not in focus were not counted for distribution measurements. Since the dispersed phase fraction was low (0.1–0.5%), film area small, it was not possible to get a larger sample especially at small times. In order to increase the accuracy of the distributions measurement, the exact diameters of the droplets were measured instead of categorizing them into class intervals.

Continuous Flow Experiments

The steady-state drop-size distributions for lean dispersions in a continuous flow vessel were measured using high speed macrophotography. The schematic diagram of the experimental setup is shown in Figure 3. The flow vessel was a 2×10^{-3} m^3 jacketted glass vessel of the same dimensions as that of the batch system. The jacket was provided to circulate water from a constant temperature water bath in order to maintain the temperature at 300 ± 0.1 K. The vessel and its water jacket were provided with aligned congruent circular optical windows for photographing the dispersion. The continuous phase was pumped from a storage tank into the flow vessel through two inlet ports. The dispersed phase was introduced into the flow vessel in the form of droplets of more or less equal size. The inlet droplets were produced by means of a hypodermic needle (of size 27G and 30G) located in the top inlet port to the vessel. The dispersed phase was pumped from a storage tank by means of a Masterflex peristaltic pump. The peristaltic pump was operated at its maximum flow rate and the dispersed phase

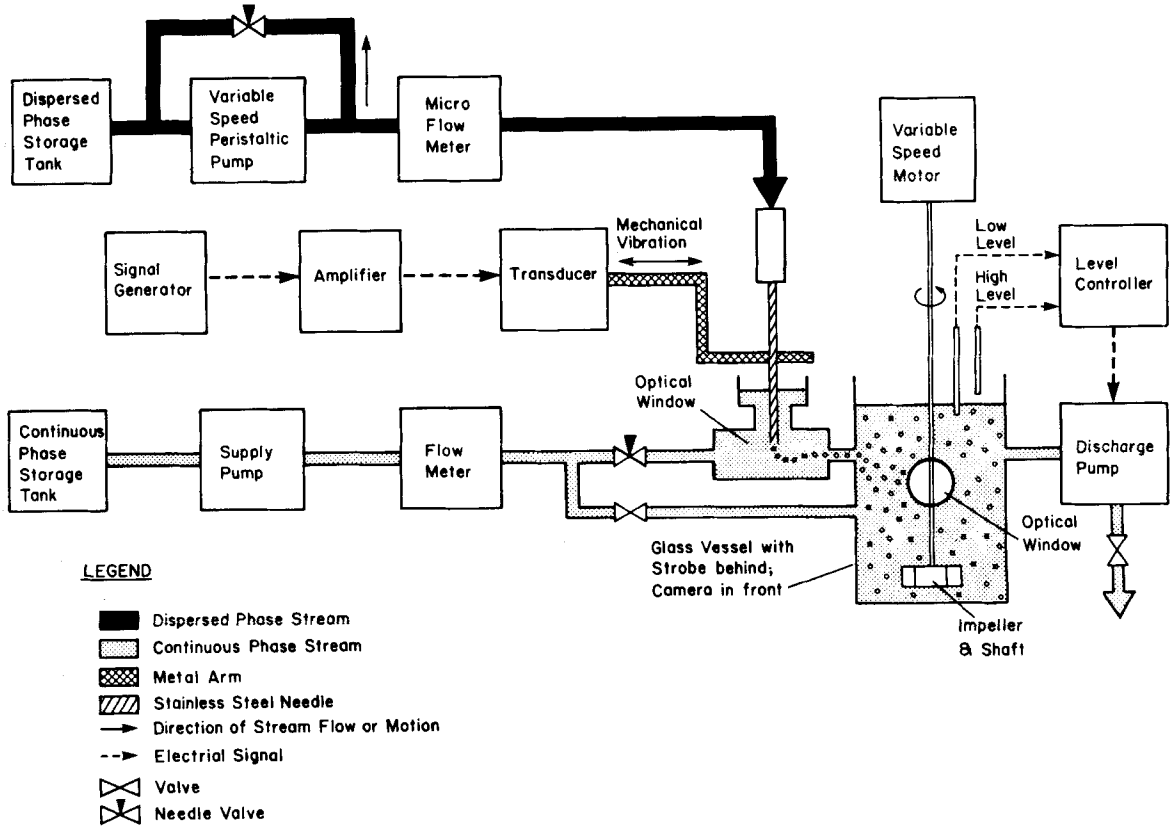

Figure 3. Schematic diagram of the continuous flow system.

flow rate was controlled by means of a needle valve in the bypass line. This ensured essentially constant dispersed phase flowrate with negligible pulsation. The hypodermic needle was mechanically connected to the transducer by a metal arm. Monodispersed droplets were formed by mechanical vibration of the drop forming hypodermic needle at a constant frequency and amplitude (Rajagopaan, 1973) by means of signal generator and transducer. Constant holdup was maintained in the vessel by means of Dynasense liquid level controller connected to the discharge pump. The dispersion was agitated by 0.05-m-diameter six-blade turbine impeller driven by Fischer stedi speed motor with speed control.

Experimental Procedure

Prior to each experiment, the flow vessel was cleaned thoroughly with chromic acid and purged with distilled water to remove traces of chromic acid. Continuous phase was then pumped from the storage tank through the flowmeter into the vessel. The impeller speed was then set and measured by means of stroboscope. The stainless-steel hypodermic needle was then inserted into the metal arm and positioned in the top inlet port. Before commencing the dispersed phase flow, the metal arm was vibrated at around 400 Hz with an amplitude of about 10^{-4} m. The dispersed phase flow was then started and the flow rate controlled by the needle valve in the bypass line. Positioning of the tip of the drop forming needle in the inlet port was found to be critical for the formation of drops of equal size. The continuous-phase input was divided into the inlet ports such that a certain minimum velocity was maintained in the top port in order to carry the drops into the vessel. Care was taken to restrict the flow rate through the top port below a maximum to avoid turbulence and subsequent breakage of drops at the inlet. The system was allowed to run at least for five average residence times to ensure the attainment of steady state. Photographs of the dispersion were then taken with Olympus OM-2(N) camera with autobellows at a magnification of 1. The dispersion was illuminated by high speed flash and a flash delay of around 20 nanoseconds was used to synchronise the flash and the shutter opening at a shutter speed of 1/100 s. Several photographs were taken to verify the attainment of steady state. The camera was focused on the droplets near the optical window. The camera and the stroboscope were then repositioned to photograph the inlet droplets in order to measure the inlet drop-size distribution. Photographs were then analyzed by means of Eyecom image processing system with PDP-11 microprocessor for drop size distribution measurements. It was possible to enhance the contrast of the image using image processing to obtain better quality images for analysis. Around 300 droplets were analyzed for each distribution measurement.

EXPERIMENTAL RESULTS AND DISCUSSION

Batch Experiments

Transients of drop-size distributions in batch agitated lean liquid-liquid dispersions were measured for three dispersed phases. The different systems and experimental conditions are given in Table 1. Most of the experiments were conducted at the dispersed phase fraction of 0.2%. Measurements were also made at dispersed phase fractions of 0.1 and 0.5% to study the effect of dispersed phase fraction. The dispersed phase fractions did not have a significant effect according to Kolmogorov-Smirnov two sample tests, thus indicating that coalescence was negligible. The reproducibility of measurement was tested through Kolmogorov-Smirnov two sample tests which showed that the experiments were reproducible. Figure 4 gives the typical plot of cumulative drop volume distribution function $F(v,t)$ vs. drop diameter at various times.

Similarity Test

Figure 5 gives the typical plot of stirring time vs. drop volume for different fixed cumulative volume percents for the above measurements. (Figure 5 is representative of similar plots which were obtained for all the systems and experimental conditions. They are not presented here for conciseness of presentation.) The solid curves in Figure 5 indicate the curves fitted to the experimental points through least squares.

TABLE 1. SYSTEMS AND EXPERIMENTAL CONDITIONS

System	Agitator Speed (s^{-1})
Water-Chlorobenzene	5, 6.67, 8.33
Water-CCl_4 + i-Octane (0.5–0.5)	5, 6.67, 8.33
Water-Anisole + CCl_4 (0.8–0.2)	5, 6.67, 8.33

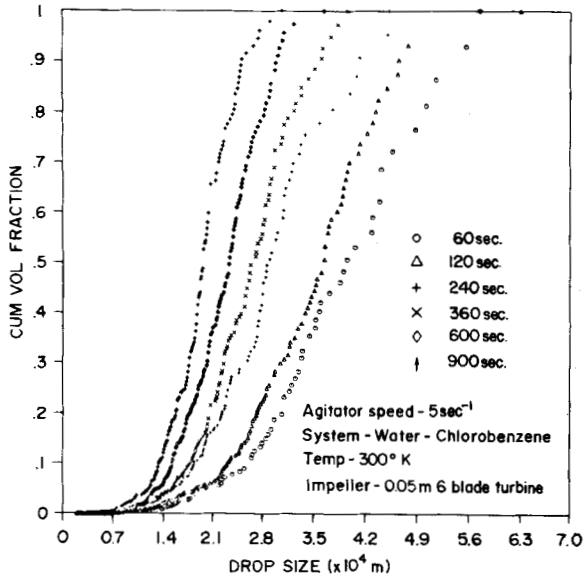

Figure 4. Effect of stirring time on drop-size distribution.

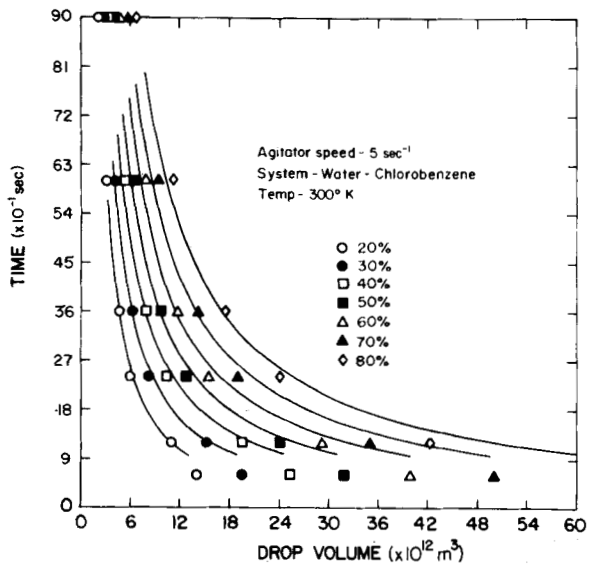

Figure 5. Plot of stirring time vs. drop volume for fixed cumulative volume percents.

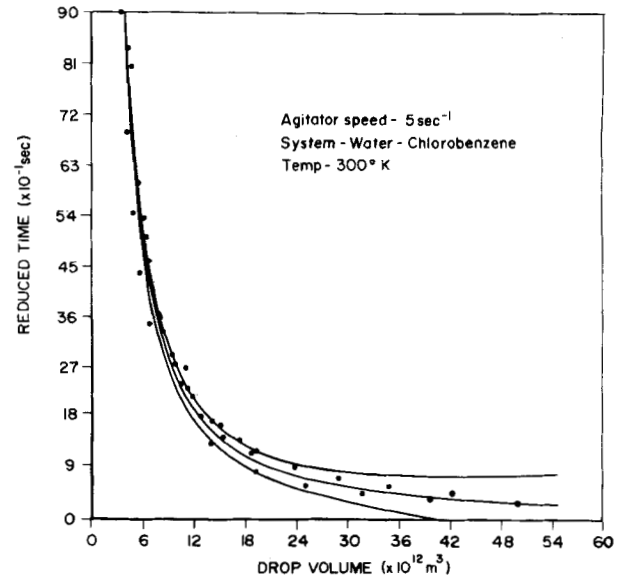

Figure 6. Plot of reduced time vs. drop volume.

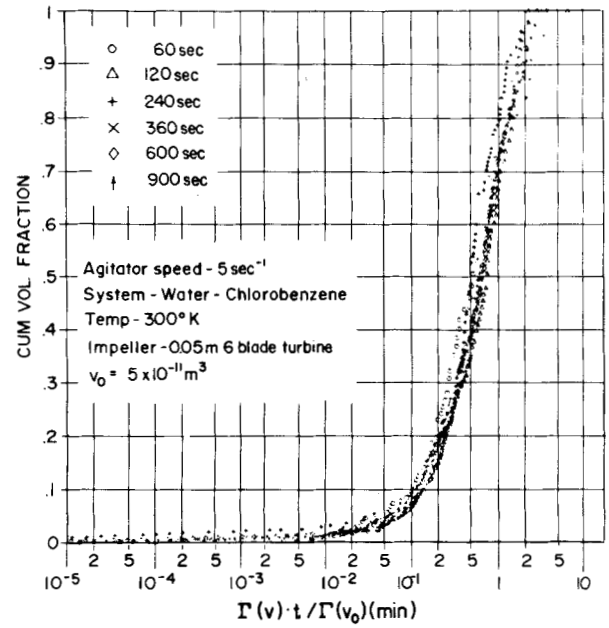

Figure 7. Plot of cumulative volume fraction versus similarity variable $\Gamma(v)\cdot t/\Gamma(v_o)$.

As discussed early, it is possible to collapse the above plots through simple translation if similarity holds. The details of the numerical procedure for translation of the t vs. v plots are given elsewhere (Narsimhan et al., 1980). Figure 6 gives a typical translated plot of stirring time vs. drop volume. The solid lines indicate the least square fit of the collapsed experimental data along with 90% upper and lower confidence limits. The experimental points do collapse into a single curve thus upholding similarity. There seems to be more scatter at small times or large droplet volumes. This is in part due to experimental errors because of smaller sample size for distribution measurement at small stirring times. Another possible explanation is that a similar distribution is attained only in course of time.

The fitted curves in Figure 6 was used to estimate $\Gamma(v)/\Gamma(v_o)$ as given by Eq. 6. The estimated transitional breakage probability $\Gamma(v)/\Gamma(v_o)$ is used to transform the drop volume distributions $F(v,t)$ at different times under the transformation $z' = \Gamma(v)t/\Gamma(v_o)$. Figure 7 gives a representative plot of $f(z')$ vs. z' for one experimental case. The transformed distributions do collapse into a single curve thus upholding similarity. The agreement seems to be excellent in all the cases excepting for water-chlorobenzene at agitator speeds of 6.67 s^{-1} and 8.33 s^{-1}. The transformed drop volume distributions at large stirring times seem to show some scatter in case of water-chlorobenzene system at the agitator speeds of 6.67 s^{-1} and 8.33 s^{-1}. This is believed to be due to errors involved in the estimation of $\Gamma(v)/\Gamma(v_o)$ for very small drop volumes. The t vs. v curves rise very steeply for small drop volumes due to rapid decrease in the rate of breakage. The fitted curve to the collapsed experimental points of reduced time vs. v seem to show smaller confidence intervals in the region where it rises sharply, i.e., small drop volumes. This makes the estimation of $\Gamma(v)/\Gamma(v_o)$ less reliable for small drop volumes.

Daughter Droplet-Size Distribution

The daughter droplet-size distribution $g(x)$, and $\Gamma(v_o)$ were estimated through the use of trial functions as given in Eq. 12 by an unconstrained multivariable optimization scheme (see Appendix 1 for details) using the moments $\{\mu_n\}$ estimated from the similarity plots of $\bar{f}(z)$ vs. z. Because of the nonlinear nature of the objective function, the optimization procedure yielded multiple solutions for the values of the parameters $\Gamma(v_o, r, s$ and x_o with a small variation in the objective function. The multiple solutions represented distributions falling into a small band with a variation in the estimated values of $\Gamma(v_o)$ of the order of ±18%. The solution corresponding to the minimum value of the objective function was chosen as the "true" solution. The values of estimated $\Gamma(v_o)$ are given in Table 2. Figure 8 gives the plots of estimated daughter droplet-distribution functions $g(x)$. The estimated daughter droplet distribution functions in all the cases seem to be similar with the value of x_o varying from 0.5 to 0.63. The parameters

TABLE 2. ESTIMATED VALUES OF TRANSITION BREAKAGE PROBABILITY

System	Agitator Speed (s^{-1})	v_o ($\times 10^{12} m^3$)	$\Gamma(v_o)$ ($\times 10^2 s^{-1}$)
Water-Chlorobenzene	5	50	5.68
Water-Chlorobenzene	6.67	60	40.80
Water-Chlorobenzene	8.33	15	42.48
Water-Anisole + CCl_4 (0.8-0.2)	5	35	11.50
Water-Anisole + CCl_4 (0.8-0.2)	6.67	20	21.89
Water-Anisole + CCl_4 (0.8-0.2)	8.33	10	7.18
Water-CCl_4 + i-Octane (0.5-0.5)	5	500	22.73
Water-CCl_4 + i-Octane (0.5-0.5)	6.67	100	13.50
Water-CCl_4 + i-Octane (0.5-0.5)	8.33	30	19.40

TABLE 3. PARAMETERS OF DAUGHTER DROPLET-DISTRIBUTION FUNCTION

Dispersed Phase	Agitator Speed (s^{-1})	r	s	x_o
Chlorobenzene	5	1.0236	1.0236	0.6094
	6.67	1.047	1.047	0.5189
	8.33	1.047	1.047	0.5189
Anisole + CCl_4	5	1.047	1.047	0.5189
(0.8-0.2)	6.67	2.094	2.094	0.6377
	8.33	1.047	1.047	0.5189
CCl_4 + i-Octane	5	1.094	1.236	0.5236
(0.5-0.5)	6.67	2.047	2.047	0.5189
	8.33	1.094	1.094	0.5377
Fitted Curve		1.3816	1.1971	0.50254

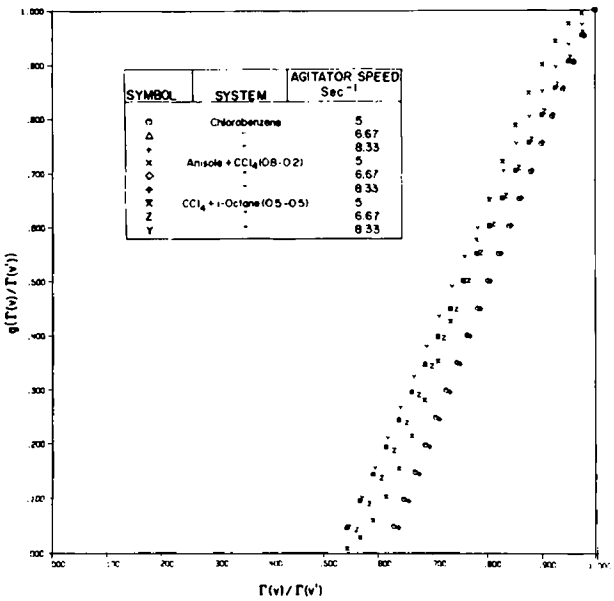

Figure 8. Nondimensionalized plot of daughter drop distribution.

of the estimated daughter droplet distribution functions and the fitted distribution functions are listed in Table 3. The estimated daughter droplet distribution functions are correlated by,

$$g(x) = \begin{cases} 0 & x < 0.50 \\ 3.01 \int_{0.50}^{x} (y - 0.50)^{0.38} (1 - y)^{0.20} \, dy \end{cases}$$

with an error of 19.96%.

The estimated functions $g(x)$ were transformed to $G(v,v')$ using the estimated values of $\Gamma(v)/\Gamma(v')$. Figure 9 shows a typical plot of $G(v,v')$ vs. v/v' for different values of parent droplet volume v'. It can be seen that the function $G(v,v')$ shifts towards smaller values of v/v' as v' increases. This is consistent with the concept of similarity proposed earlier.

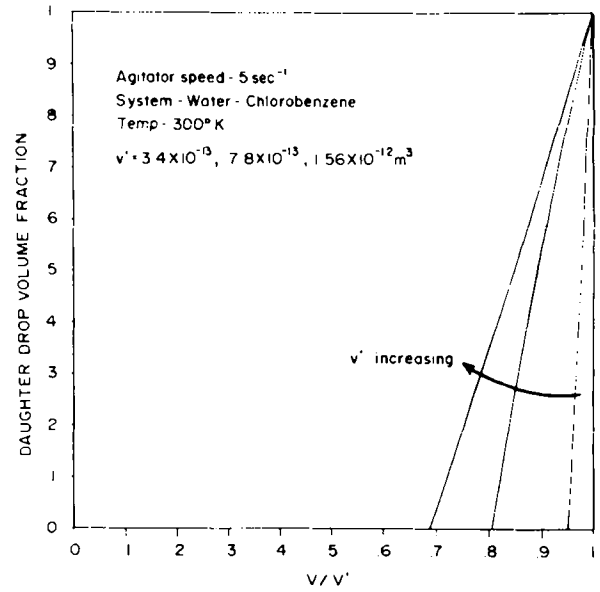

Figure 9. Plot of $G(v,v')$ vs. v/v'.

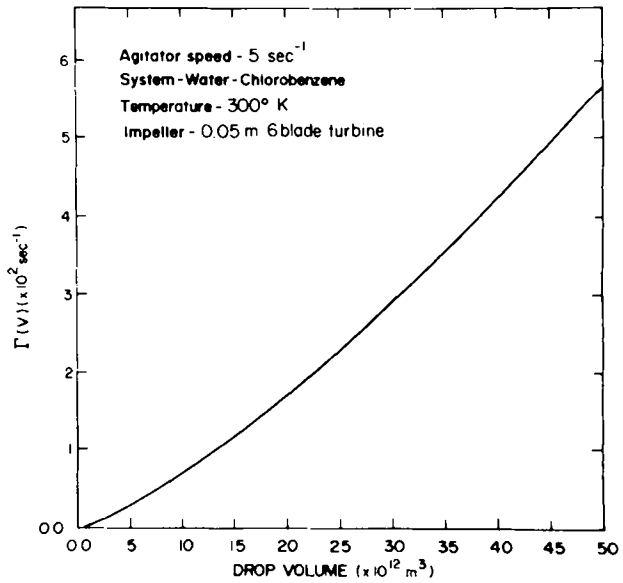

Figure 10. Plot of transitional breakage probability.

Transition Breakage Probabilities

With the knowledge of $\Gamma(v)/\Gamma(v_o)$ and the estimates of $\Gamma(v_o)$, it is now possible to evaluate the magnitude of transitional breakage probabilities as a function of droplet volume. Figure 10 gives a typical plot of estimated transition breakage probability.

From dimensional analysis, it can be shown that the transitional breakage probability for various systems and experimental conditions could be collapsed into a single curve as a plot of

$$\Gamma(v)\sqrt{\frac{\rho v}{\sigma}} \text{ vs } We\left(\frac{v}{L^3}\right)^{5/9}$$

where $\sqrt{\sigma/\rho v}$ is proportional to the natural frequency of oscillation of a droplet of volume v. Figure 11 shows the nondimensional plot. The estimated values of transitional probability do collapse approximately into a single curve. The scatter may be attributed to the uncertainty in the estimated values of $\Gamma(v_o)$ due to the existence of multiple solutions. The importance of this plot lies in its usefulness in the estimation of transitional breakage probability of a droplet of volume v from the physical properties of the system and the experimental conditions. The experimental data were correlated by the following equation,

$$\Gamma(v)\sqrt{\frac{\rho v}{\sigma}} = 5.75\, We^{3.2}\left(\frac{v}{L^3}\right)^{1.78}$$

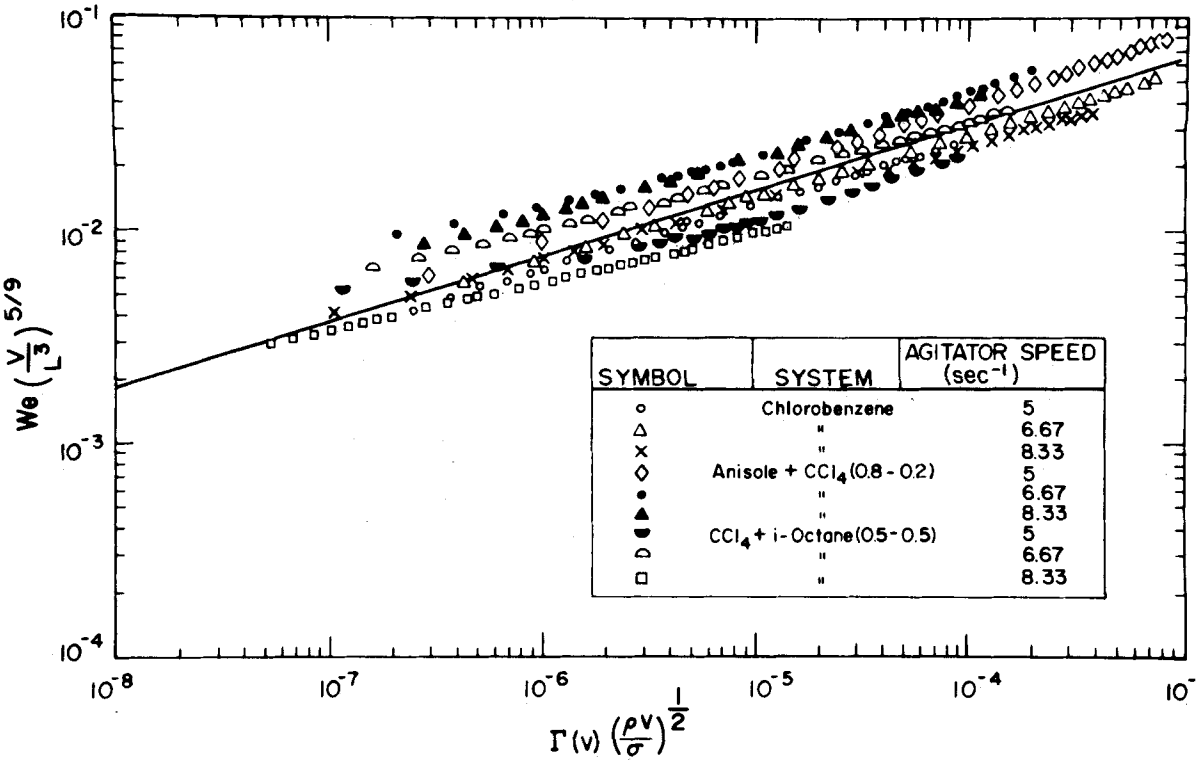

Figure 11. Nondimensional plot of transitional breakage probability.

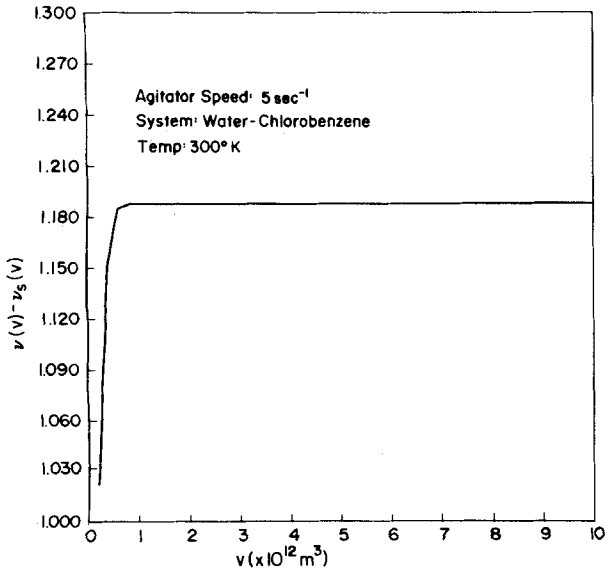

Figure 12. Plot of "mean number of daughter droplets" vs. drop volume.

The correlation coefficient was found to be 0.926 and the correlation was found to explain 85.78% of the total variation.

Mean Number of Daughter Droplets

The function $\nu(v') - \nu_s(v')$ was determined from the knowledge of $g(x)$ and $\Gamma(v')$ using Eq. 16. Figure 12 gives the typical plot of estimated $\nu(v') - \nu_s(v')$ vs. v'. The 'mean number' of daughter droplets approaches 1 as $v \to v_s$. It increases rapidly near v_s and tapers off to a value between 1 and 2 for large drop volumes. This indicates that breakage may be "erosive" for the droplet ranges encountered in the experiments which is consistent with the nature of estimated $g(x)$.

Continuous Flow Experiments

Steady-state drop-size distributions in a continuous-flow system were measured for two dispersed phases and three different agitator speeds. The average residence time was varied in the range of 60 sec to 360 s. Residence time distribution measurements were made from the response to both pulse and step tracer inputs. The residence time distribution was found to be essentially that of a perfectly mixed vessel. The dispersed phase fraction was maintained at less than 0.25% in order to minimize the effect of coalescence. Though the inlet drop size distribution was maintained as a narrow distribution, the average inlet drop size varied from one experiment to another in the range of 250 to 450 microns. Kolmogorov-Smirnov two-sample tests indicated that the experiments were reproducible. Different systems and experimental conditions are given in Table 4.

TABLE 4. EXPERIMENTAL RUNS FOR CONTINUOUS FLOW SYSTEM

Dispersed Phase	Agitator Speed (s^{-1})	Average Residence Time (s)	Dispersed-Phase Fraction (%)	Inlet Droplet Size μm)
Chlorobenzene	5	55	0.07	454 ± 46
		70	0.06	360 ± 40
		85	0.19	*
		128	0.06	299 ± 30
		185	0.12	260 ± 48
		248	0.14	290 ± 35
		319	0.22	324 ± 60
		355	0.24	367 ± 45
Chlorobenzene	6.67	88	0.14	457 ± 32
		183	0.13	374 ± 64
		272	0.18	323 ± 47
		355	0.24	417 ± 47
		363	0.20	304 ± 26
Chlorobenzene	8.33	89	0.17	485 ± 63
		183	0.13	357 ± 39
		272	0.18	305 ± 38
		363	0.20	308 ± 15
CCl_4 + i-Octane (0.5–0.5)	8.33	85	0.15	331 ± 68
		187	0.18	341 ± 37
		271	0.23	480 ± 70
		322	0.24	510 ± 81

* Very large inlet droplets.

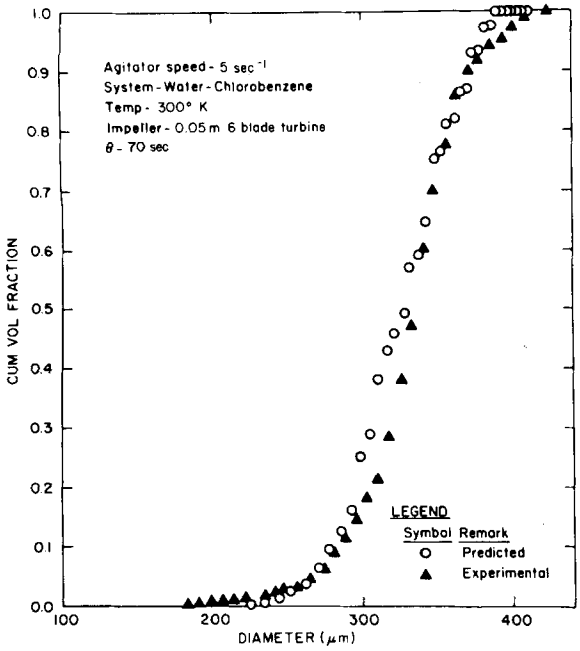

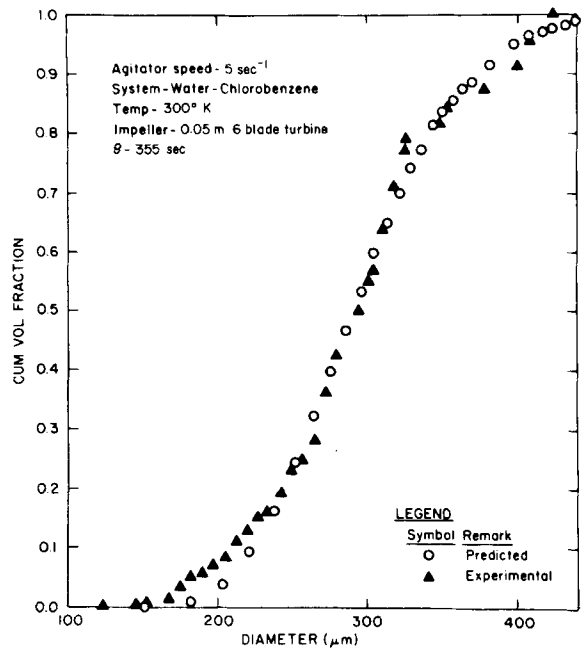

Figures 13–14. Comparison of experimental and predicted steady-state drop-size distributions.

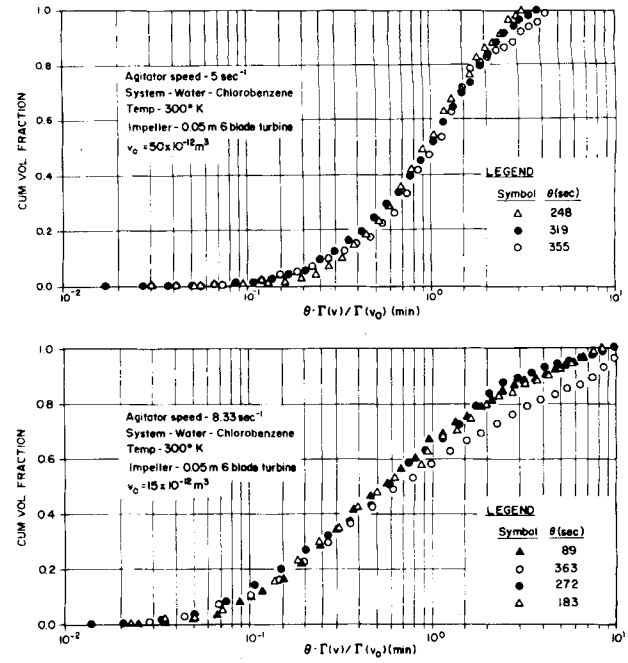

Figures 15–16. Plot of steady-state drop-volume distribution function vs. similarity variable $\theta\Gamma(v)/\Gamma(v_o)$.

Comparison with Predicted Distributions

Steady-state drop-size distributions were predicted through the solution of the population balance equation (Eq. 17) using the measured inlet drop-size distribution. The numerical scheme for the solution of Eq. 17 was outlined earlier. The transition breakage probability function $\Gamma(v)$ and the daughter droplet distribution function $g(\Gamma(v)/\Gamma(v'))$ estimated from batch experiments were used for the prediction of the steady-state drop-size distributions. (The breakage functions estimated from the batch experiments for the particular system and operating conditions were used for the prediction rather than the generalized correlations.) Consequently when the feed drop sizes were not of the size range for which the breakage probabilities had been determined, successful prediction of the steady state drop size distribution cannot be expected. This was the case for the experiments with water-chlorobenzene at the agitator speed of 8.33 s^{-1}. The predicted steady-state drop-size distributions generally compare well with the experimental distributions. The comparisons were found to be especially good for the system of water-chlorobenzene at the agitator speed of 5 s^{-1}. Any discrepancy between the experimental and predicted distributions was found to be more pronounced for large inlet drop sizes. This discrepancy can be attributed partly to the errors involved in the measurement of inlet drop-size distribution since only around 60 droplets were counted for each inlet drop-size distribution measurement. Typical comparison between the experimental and predicted distributions are shown in Figures 13 and 14. Kolmogorov-Smirnov one-sample test was successfully performed in order to make quantitative comparison between the experimental and predicted steady state distributions.

Test of Similarity

As discussed earlier, one can expect similarity behavior in continuous-flow systems when the average residence times is much larger than: (i) the time scale for attainment of similarity and (ii) the time scale of breakage of inlet drops. In order to verify the existence of similarity behavior, the experimental steady-state drop-size distributions at different average residence times were plotted as a function of $\theta\Gamma(v)/\Gamma(v_o)$, where v_o is some reference drop volume. It was found that the distributions collapsed into a single curve whenever $\Gamma(v_f)\theta$ was greater than 2.5, where v_f refers to the inlet drop volume that is one standard deviation less than the average of the inlet distribution. Typical similarity plots for different systems and agitator speeds are given in Figures 15 and 16. The distributions exhibit some scatter in the cumulative volume fraction range of 0–9 to 1.0 because of difference among the inlet drop-size distributions. The similarity behavior is found to be excellent in all the cases excepting for the system of water-chlorobenzene at the agitator speed of 8.33 s^{-1} especially at the average residence time of 363 s.

IN CONCLUSION

The experimental data on the transients of drop-size distribution in a batch stirred liquid-liquid dispersion uphold the similarity hypothesis proposed by Narsimhan et al. (1980). The estimated rate functions for drop breakage are correlated in terms of appropriate dimensionless groups. The experimental steady-state drop-size distributions in a stirred continuous flow system compare very favorably with the theoretical predictions and substantiate the proposed similarity behavior for continuous systems.

ACKNOWLEDGMENT

The authors wish to acknowledge the National Science Foundation for support of the work through NSF Research Grants ENG 77-19367 and CPE-8001749.

NOTATION

f = drop volume density, m^{-3}
F = cumulative drop volume distribution
g = cumulative daughter droplet distribution for "similar" breakage
G = cumulative daughter distribution
L = impeller diameter, m
N = agitator speed, s^{-1}
r,s = parameters of beta distribution
t = time, s
v = droplet volume, m^3
v_s = maximum stable drop volume, m^3
We = $\frac{N^2L^3\rho}{\sigma}$, Weber number
x = ratio of transitional breakage probabilities of daughter and parent droplets
x_o = parameter of beta distribution
z = similarity variable

Greek Letters

ν = mean number of daughter droplets, also used as the moments of daughter droplet distribution
μ = moments of drop volume distribution
θ = average residence time, s
Γ = transitional breakage probability, s^{-1}
τ = age, s
τ' = dimensionless age
ρ = density, kg/m^3
σ = interfacial tension, kg/m·s

Subscripts

f = feed
v = differentiation with respect to volume
n = nth moment

Superscript

$\sim$ = steady state

APPENDIX I: ESTIMATION OF $\Gamma(v_o)$ AND $g(x)$

It is of interest to estimate $\Gamma(v_o)$ and $g(x)$ from the values of $\{\Gamma(v_o)\nu_n\}$, $n = 1, 2, \ldots$ where $\{\nu_n\}$ are the constants defined as,

$$\nu_n = \int_0^1 x^n g(x)dx \tag{I.1}$$

It can be assumed that the daughter droplet distribution function $g(x)$ is zero for values of x less than x_o(say), where x_o is an unknown parameter of the distribution. Further, the distribution function is assumed to be a beta distribution in the interval $(x_o,1)$ of parameters r and s (say). The daughter droplet density can therefore be written as,

$$g'(x) = 0 \qquad x < x_o$$
$$= \frac{1}{(1-x_o)}\left(\frac{x-x_o}{1-x_o}\right)^{r-1}\left(\frac{1-x}{1-x_o}\right)^{s-1} \quad x \geq x_o \tag{I.2}$$

The nth moment of the distribution γ_n is then given by,

$$\gamma_n = \int_0^1 \{(1-x_o)y + x_o\}^n g(y)dy$$

in terms of the transformed variable $y = (x - x_o/1 - x_o)$. Therefore,

$$\gamma_n = \sum_{i=0}^{n}\int_0^1 \binom{n}{i}(1-x_o)^i y^i x_o^{n-i} g(y)dy$$
$$= \sum_{i=0}^{n}\binom{n}{i}(1-x_o)^i x_0^{n-i}\frac{\Gamma(r+s)\,\Gamma(r+i)}{\Gamma(i+t)\,\Gamma(r)}, \quad t = r+s \tag{I.3}$$

It can be easily seen that,

$$\nu_n = \frac{1}{n+1}(1-\gamma_{n+1}) \tag{I.4}$$

Therefore, given the parameters x_o, r and s of daughter droplet distribution, the estimate of $\Gamma(v_o)$ from $\{\Gamma(v_o)\nu_n\}$ is given by,

$$\hat{\Gamma}(v_o)_n = \frac{\{\Gamma(v_o)\nu_n\}(n+1)}{(1-\gamma_{n+1})} \quad n = 0, 1, 2, \ldots \tag{I.5}$$

where γ_{n+1} is given by Eq. I.3.

Therefore, the average estimate of $\Gamma(v_o)$ from the values of $\{\Gamma(v_o)\nu_n\}$ $n = 0, 1, 2 \ldots N-1$ is given by,

$$\overline{\Gamma(v_o)} = \frac{1}{N}\sum_{n=0}^{N-1}\hat{\Gamma}(v_o)_n \tag{I.6}$$

The standard deviation of the estimates of $\Gamma(v_o)$ from the constants $\{\Gamma(v_o)\nu_n\}$ is given by,

$$S.d. = \frac{1}{N}\sum_{n=0}^{N-1}\{\hat{\Gamma}(v_o)_n - \overline{\Gamma(v_o)}\}^2 \tag{I.7}$$

The parameters r, s and x_o of the daughter droplet distribution $g(x)$ are estimated by minimizing the objective function

$$\epsilon = \frac{1}{N}\sum_{n=0}^{N-1}\{\hat{\Gamma}(v_o)_n - \overline{\Gamma(v_o)}\}^2/\overline{\Gamma(v_o)}^2 \tag{I.8}$$

The Nelder and Mead algorithm for multivariable unconstrained minimization is employed for the estimation of the parameter r, s and x_o.

LITERATURE CITED

Levich, V. G., "Physico Chemical Hydrodynamics," Prentice Hall Inc. (1962).

Narsimhan, G., D. Ramkrishna, and J. P. Gupta, "Analysis of Drop Size Distributions in Lean Liquid-Liquid Dispersions," *AIChE J.*, **26**, p. 991 (1980).

Rajagopalan, F., and Chi Tien, "Production of Mono-dispersed Drops by Forced Vibration of a Liquid Jet," *Can. J. Chem. Eng.*, **51**, p. 272 (1973).

Ramkrishna, D., "Drop Breakage in Agitated Liquid-Liquid Dispersions," *Chem. Eng. Sci.*, **29**, p. 987 (1974).

Shinnar, R., "On the Behavior of Liquid Dispersions in Mixing Vessels," *J. Fluid Mech.*, **10**, p. 259 (1961).

Manuscript received May 28, 1982; revision received June 28, and accepted July 1, 1983.